Electronic states of $EuCu_2Ge_2$ and $EuCu_2Si_2$ studied by soft x-ray photoemission spectroscopy

Ikuto Kawasaki,[1,*] Shin-ichi Fujimori,[1] Yukiharu Takeda,[1] Hiroshi Yamagami,[1,2] Wataru Iha,[3] Masato Hedo,[4] Takao Nakama,[4] and Yoshichika Ōnuki[4]

[1]*Materials Sciences Research Center, Japan Atomic Energy Agency, Sayo, Hyogo 679-5148, Japan*
[2]*Department of Physics, Faculty of Science, Kyoto Sangyo University, Kyoto 603-8555, Japan*
[3]*Graduate School of Engineering and Science, University of the Ryukyus, Nishihara, Okinawa 903-0213, Japan*
[4]*Faculty of Science, University of the Ryukyus, Nishihara, Okinawa 903-0213, Japan*

(Received 4 March 2019; revised manuscript received 21 June 2019; published 12 July 2019)

We have carried out angle-integrated photoemission spectroscopy (AIPES) and angle-resolved photoemission spectroscopy (ARPES) experiments using soft x rays on single crystals of $EuCu_2Ge_2$ and $EuCu_2Si_2$ grown by the Bridgman method to investigate their electronic structures. The AIPES results showed that the Eu ions in $EuCu_2Ge_2$ and $EuCu_2Si_2$ are in a divalent state and a nearly trivalent state, respectively, in accordance with the previously reported magnetic properties. The three-dimensional band structures and shapes of the Fermi surfaces of $EuCu_2Ge_2$ and $EuCu_2Si_2$ were studied by ARPES measurements. We found that the band structures near the Fermi level and Fermi surfaces of $EuCu_2Ge_2$ and $EuCu_2Si_2$ are very different from each other and are well reproduced by the band structure calculations based on density-functional theory for $SrCu_2Ge_2$ and YCu_2Si_2. This suggests that a charge transfer from the localized $4f$ states into the valence bands is responsible for the difference in the electronic states between $EuCu_2Ge_2$ and $EuCu_2Si_2$.

DOI: 10.1103/PhysRevB.100.035111

I. INTRODUCTION

Ce- and Yb-based $4f$ electron compounds show a variety of fascinating properties, such as heavy-fermion states, non-Fermi-liquid behavior, and anisotropic superconductivity [1–4]. The $4f$ electronic states in these systems are quite sensitive to the strength of the hybridization with conduction electrons, and the magnetic ground states of the localized $4f$ electrons evolve into nonmagnetic ground states with increasing the hybridization by applying pressure or doping. Most of the aforementioned intriguing properties of the Ce- and Yb-based compounds have been observed near a quantum critical point, at which the second-order magnetic transition temperature decreases to zero, and the strong electron correlation effect and quantum fluctuations play important roles.

It has been found that Eu-based compounds also exhibit magnetic-to-nonmagnetic transitions. In the vast majority of Eu-based compounds, a magnetic divalent electronic state ($4f^7$: $S = 7/2$, $L = 0$, and $J = 7/2$) is stable compared to a nonmagnetic trivalent state ($4f^6$: $S = 3$, $L = 3$, and $J = 0$), unlike the Ce- and Yb-based compounds, where the rare-earth atoms are usually trivalent. Here, S, L, and J represent the spin, orbital, and total angular momentum, respectively. Interestingly, the energy difference between the Eu divalent (Eu^{2+}) state and Eu trivalent (Eu^{3+}) state is very small. Because Eu^{3+} ions are smaller than Eu^{2+} ions, valence and magnetic-to-nonmagnetic transitions can be induced by external and chemical pressure. In fact, valence transitions from a magnetic Eu^{2+} state to a nonmagnetic nearly Eu^{3+} state occur upon the application of pressure in several Eu-based compounds, such as $EuRh_2Si_2$ [5,6], $EuNi_2Ge_2$ [7,8], $EuCo_2Ge_2$ [9], and $EuGa_4$ [10]. The variation of the magnetic transition temperature with pressure in these compounds is markedly different from that in Ce- and Yb-based compounds, and the magnetic order disappears abruptly at critical pressure, at which valence transitions occur. Above the critical pressure, these compounds exhibit temperature-induced valence transitions, which seem to be of first order.

In contrast to these Eu compounds, the variation of the magnetic transition temperature of $EuCu_2(Ge_{1-x}Si_x)_2$ with x is similar to that of Ce- and Yb-based compounds [11,12] and is reminiscent of the Doniach phase diagram [13]. $EuCu_2Ge_2$ is a nearly divalent system and exhibits an antiferromagnetic phase transition at around 14 K; the effective magnetic moment estimated from the susceptibility is close to the value for a free Eu^{2+} ion. The Néel temperature increases slightly with x, showing a maximum at around $x = 0.5$, and then it decreases rapidly for $x \geqslant 0.5$. No magnetic transition is observed above the critical concentration $x_c = 0.65$. Inelastic neutron scattering experiments showed that quasielastic magnetic excitations disappear gradually around x_c with increasing x, which reflects a quenching of magnetic moments in the ground state, and that a spin gap is formed in the excitation spectra for $x \geqslant 0.8$ at low temperatures [14,15]. X-ray absorption spectroscopy (XAS) and Mössbauer experiments revealed that the Eu valence is stable and close to Eu^{2+} for $x \leqslant 0.5$, whereas the Eu valence evolves continuously toward Eu^{3+} for $x \geqslant 0.5$ [11,15,16]. Here, it should be emphasized that although the valence state of the end material $EuCu_2Si_2$ is close to a Eu^{3+} state, this compound remains in a mixed-valence state. One of the striking features of $EuCu_2(Ge_{1-x}Si_x)_2$ is the emergence of the heavy-fermion

*kawasaki.ikuto@jaea.go.jp

behavior around x_c. The electronic specific-heat coefficient γ reaches approximately 300 mJ K^{-2} mol^{-1} around x_c, and the quadratic term in the resistivity and the temperature-independent susceptibility are also enhanced in the same x range, indicating the presence of heavy quasiparticles at low temperatures [11,12]. Above x_c, γ decreases rapidly as x approaches 1. These results clearly show that the electronic and magnetic properties of $EuCu_2(Ge_{1-x}Si_x)_2$ for $x \geqslant 0.5$ evolve dramatically with x and cannot be understood in terms of an atomiclike picture, which assumes simple superposition of the Eu^{2+} and Eu^{3+} ionic states. Therefore, the hybridization between the $4f$ and the conduction electrons plays a crucial role.

All of the electronic and magnetic properties of $EuCu_2(Ge_{1-x}Si_x)_2$ mentioned above have been clarified by experiments performed on arc-melted polycrystals. Thus far, several groups have synthesized single crystals of $EuCu_2Ge_2$ and $EuCu_2Si_2$ by the In-flux method [17–20]. The electronic and magnetic properties of the In-flux-grown single crystals of $EuCu_2Ge_2$ are very similar to those of the arc-melted polycrystals, despite the former samples exhibiting a lower Néel temperature than the latter samples. On the other hand, magnetic susceptibility and Mössbauer experiments have demonstrated that the In-flux-grown single crystals of $EuCu_2Si_2$ have a stable Eu^{2+} state and exhibit a spin-glass-like order at low temperatures, in stark contrast to arc-melted polycrystals, which exhibit mixed-valence behavior and are nonmagnetic [20]. It has been found by the x-ray powder diffraction and Laue method that the In-flux-grown single crystals of $EuCu_2Si_2$ have a larger unit-cell volume and possess crystal defects [20,21]. These are considered to be reasons for their spin-glass order and Eu^{2+} state. Recently, we succeeded in growing single crystals of $EuCu_2(Ge_{1-x}Si_x)_2$ by the Bridgman method [21]. The lattice parameters of the Bridgman-grown single crystals are nearly of the same magnitude as those of the arc-melted polycrystals, and the electronic and magnetic properties, including the heavy-fermion behavior around x_c, are very similar between them.

The magnetic-to-nonmagnetic transition and heavy-fermion behavior in $EuCu_2(Ge_{1-x}Si_x)_2$ coincide with the rapid change in Eu valence with x from the Eu^{2+} state for $EuCu_2Ge_2$ to the nearly Eu^{3+} state for $EuCu_2Si_2$. Therefore, to further understand the origin of these phenomena, it is essential to clarify the electronic structures of $EuCu_2Ge_2$ and $EuCu_2Si_2$ as well as the differences between them. To this end, we performed angle-integrated photoemission spectroscopy (AIPES) and angle-resolved photoemission spectroscopy (ARPES) experiments using bulk-sensitive soft x-ray photons [22,23] on single crystals of $EuCu_2Ge_2$ and $EuCu_2Si_2$ grown by the Bridgman method. We derived the three-dimensional band structure and Fermi surfaces (FSs) of both the compounds and compared them with the results of band structure calculations. Moreover, we also performed AIPES experiments on In-flux-grown single crystals of $EuCu_2Ge_2$ and $EuCu_2Si_2$ for comparison.

II. EXPERIMENTAL DETAILS

Single crystals of $EuCu_2Ge_2$ and $EuCu_2Si_2$ were grown by the Bridgman method as well as the In-flux method. The details of sample preparation and characterization are described in Ref. [21]. The photoemission experiments were performed at the soft x-ray beamline BL23SU [24] at SPring-8 at photon energies ranging from 650 to 800 eV, and the energy resolution was set to about 100–140 meV. The energy and angular distributions of photoelectrons were measured using a Gammadata-Scienta SES2002 analyzer. The angular resolution along the analyzer slit was $\pm 0.15^\circ$. The Fermi level E_F position was determined by the Fermi edge of an evaporated gold film. We employed a free-electron final state model with an inner potential value of $V_0 = 12$ eV to calculate the position of the ARPES scan in momentum space [25]. Clean sample surfaces parallel to the (001) plane were prepared by cleaving *in situ* just before the measurements. The base pressure of the sample chamber was maintained below 9×10^{-9} Pa throughout the measurements. The sample temperature was set to 20 K.

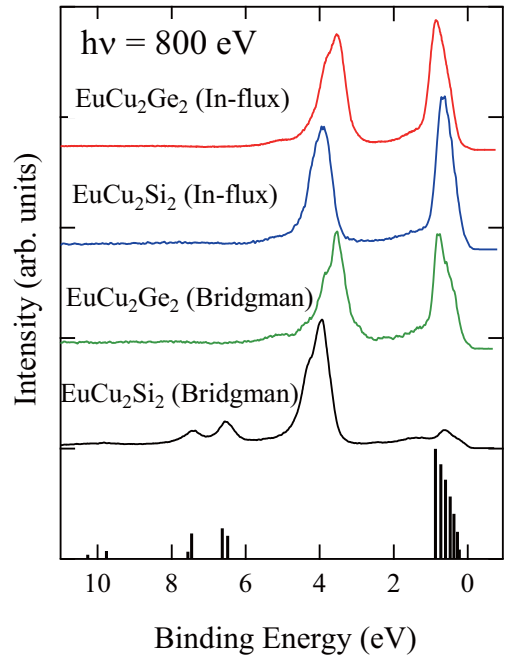

FIG. 1. AIPES spectra measured at $h\nu = 800$ eV for $EuCu_2Ge_2$ and $EuCu_2Si_2$ samples grown by the Bridgman method and those grown by the In-flux method. These spectra are normalized by the integrated intensity from 5 to 2 eV, which roughly corresponds to the total intensity of the Cu $3d$ peak. The vertical bars represent the calculated $4f^6$ and $4f^5$ final-state multiplets cited from Refs. [12,26], which correspond to the Eu^{2+} and Eu^{3+} states, respectively. The calculated $4f^6$ final-state multiplet, which is located near E_F, is shifted to match the Eu^{2+} components of the Bridgman-grown $EuCu_2Ge_2$ sample, and the calculated $4f^5$ final-state multiplet seen below 6 eV is shifted to match the Eu^{3+} components of the Bridgman-grown $EuCu_2Si_2$ sample.

III. RESULTS AND DISCUSSION

Figure 1 shows the AIPES spectra of the $EuCu_2Ge_2$ and $EuCu_2Si_2$ single crystals grown by the Bridgman method measured at $h\nu = 800$ eV. The AIPES spectra of the In-flux-grown single crystals are displayed as well. The sample temperatures were kept at 20 K, and thus, all samples were in the paramagnetic state. At this photon energy, the contributions of the Eu $4f$ and Cu $3d$ orbitals are dominant

because they are more than one order of magnitude greater than those of other states, such as Eu $5d$, Si $3p$, and Ge $4p$ [27]. The pronounced peak located at around 3–4 eV that is seen in all spectra originates from Cu $3d$-derived bands, and all spectra are normalized by the intensity of this peak. It is known that Eu^{2+} components arising from the $4f^6$ final-state multiplet are usually located between E_F and 2 eV, and Eu^{3+} components arising from the $4f^5$ final-state multiplet are located between 6 and 11 eV [12,28]. The results of atomic calculations of the $4f^6$ and $4f^5$ final-state multiplets are shown by vertical bars [12,26]. A pronounced peak due to the Eu^{2+} components is observed in the spectra of the $EuCu_2Ge_2$ sample grown by the Bridgman method and the spectra of the In-flux-grown samples. A small shoulder at the higher-binding side of this peak originates from the Eu^{2+} ions in the surface region [12]. The presence of the pronounced Eu^{2+} peak in these samples is consistent with the reported divalent nature of Eu ions in these samples [17–21]. The positions of these Eu^{2+} peaks are very close to E_F, which means that the $4f^6$ final state is nearly degenerated in energy with the $4f^7$ initial state. This is the origin of the mixed-valence behavior of $EuCu_2(Ge_{1-x}Si_x)_2$. Moreover, we found that the positions of the Eu^{2+} peaks differ depending on the sample. The peak positions are 0.85, 0.79, and 0.66 eV for the In-flux- and Bridgman-grown $EuCu_2Ge_2$ samples and the In-flux-grown $EuCu_2Si_2$ sample. This tendency can be explained by the difference in unit-cell volumes, which are 182.7, 180.2, and 168.2 $Å^3$, respectively, for these samples, because the Eu^{2+} state tends to be stabilized with increasing unit-cell volume [21]. Note that no Eu^{3+} components are seen in the spectra of these divalent samples within the experimental accuracy. This implies that although the Eu^{2+} and Eu^{3+} states are nearly degenerated in these samples, the perturbation effects, which mix different valence states, are weak, and the ground and first excited valence states are a nearly pure divalent state and a pure trivalent state, respectively.

In the AIPES spectrum of the Bridgman-grown single crystal of $EuCu_2Si_2$, the Eu^{2+} peak is significantly suppressed, and Eu^{3+} components are present below 6 eV. The coexistence of the Eu^{2+} and Eu^{3+} components reflects the mixed-valence nature of this sample. Notably, this spectrum is very different from that of previous x-ray photoemission spectroscopy measurements performed on arc-melted polycrystals of $EuCu_2Si_2$, in which a pronounced Eu^{2+} peak was observed despite its nearly trivalent Eu state [12]. This difference could be ascribed to the difference in the preparation method of the sample surfaces, and the Eu ions in the subsurface region in the previous measurements might have been shifted toward a Eu^{2+} state. We estimated the Eu valence of the present Bridgman-grown sample of $EuCu_2Si_2$ as 2.79 from the intensity of the Eu^{2+} components under the assumption that the Bridgman-grown $EuCu_2Ge_2$ sample is in a pure divalent state, and the relative population of the Eu^{2+} state is proportional to the intensity of the Eu^{2+} components. This valence value is very close to that estimated by XAS measurements performed on the arc-melted samples [11,15].

Despite the agreement on the Eu valence of $EuCu_2Si_2$ between the present AIPES and previous XAS measurements [11,15], they are not totally consistent with each other. Contrary to our AIPES results, a small but noticeable Eu^{3+} component was observed for $EuCu_2Ge_2$ in the previous XAS measurements, suggesting that the Eu ions are not in a pure divalent state but in a mixed-valence state with an estimated valence of about 2.2 at low temperatures [11,15]. It has been pointed out that this valence value seems to contradict the pure-divalent-like behavior of $EuCu_2Ge_2$ observed in the magnetization and magnetic susceptibility measurements [11,12,15]. Therefore, it was argued in the previous XAS studies that the Eu^{3+} components observed in $EuCu_2Ge_2$ can possibly be ascribed to the final-state effect and could thus be extrinsic [15]. The absence of measurable Eu^{3+} components in our AIPES spectra of the Bridgman-grown $EuCu_2Ge_2$ sample supports the pure divalent nature indicated by the magnetization and magnetic susceptibility.

To further understand the electronic states of $EuCu_2Ge_2$ and $EuCu_2Si_2$ and the difference between them, we performed ARPES experiments on the single-crystalline samples of $EuCu_2Ge_2$ and $EuCu_2Si_2$ grown by the Bridgman method. The body-centered tetragonal Brillouin zone in the paramagnetic phase is shown in Fig. 2(a). Figures 2(b) and 2(c) show the intensity plots of the ARPES spectra of $EuCu_2Ge_2$ and $EuCu_2Si_2$ at 20 K measured along the high-symmetry lines. The ARPES spectra in the Γ-X-Z plane, shown by the green plane in Fig. 2(a), were obtained by ARPES measurements at constant photon energies of $h\nu = 680$ and 710 eV for $EuCu_2Ge_2$ and $EuCu_2Si_2$; these photon energies correspond to a k_z value of $\sim$22 (in units of $2\pi/c$). The ARPES spectra along the Γ-(Λ)-Z line were obtained from $h\nu$-dependent ARPES measurements from 670 to 740 and 694 to 778 eV for $EuCu_2Ge_2$ and $EuCu_2Si_2$, respectively. The ARPES spectra shown in Figs. 2(b) and 2(c) are normalized by the integrated intensity of each energy distribution curve. The weakly dispersive bands at around 3.5–4.5 eV with strong intensities seen in both samples are Cu $3d$-derived bands. The flat feature near E_F arises from the $4f^6$ final-state multiplet, whose intensity is suppressed significantly for $EuCu_2Si_2$, as in the AIPES spectra. Several highly dispersive bands can be seen in the spectra of both samples; the structures of these dispersive bands are very similar between $EuCu_2Ge_2$ and $EuCu_2Si_2$. For example, a parabolic feature, which exhibits a minimum at 5.5–6 eV at the Γ point, is observed for both samples, as indicated by the red dashed lines. The energy position of this feature moves toward E_F while approaching the Z point in both samples. Moreover, we observe a dispersive feature, which exhibits a broad bottom at around 2.5 eV, on the Z-X line in both Figs. 2(b) and 2(c).

As mentioned above, there is a similarity between the band structures of $EuCu_2Ge_2$ and $EuCu_2Si_2$. However, we observed a clear difference between them near E_F, as shown below. The ARPES spectra of $EuCu_2Ge_2$ and $EuCu_2Si_2$ along the Γ-(Σ)-Z line measured at $h\nu = 680$ and 710 eV are shown in Figs. 3(a) and 3(b), respectively. These ARPES spectra are normalized by the integrated intensity of each momentum distribution curve. Under this normalization, the intensity of weakly dispersive features, such as the Eu^{2+} components and some Cu $3d$-derived bands, are suppressed, and therefore, this normalization allows us to investigate the details of the dispersive bands since they exhibit clear peaks in the moment distribution curves. The Fermi-edge-cutoff effect is also removed by this normalization because the Fermi-Dirac

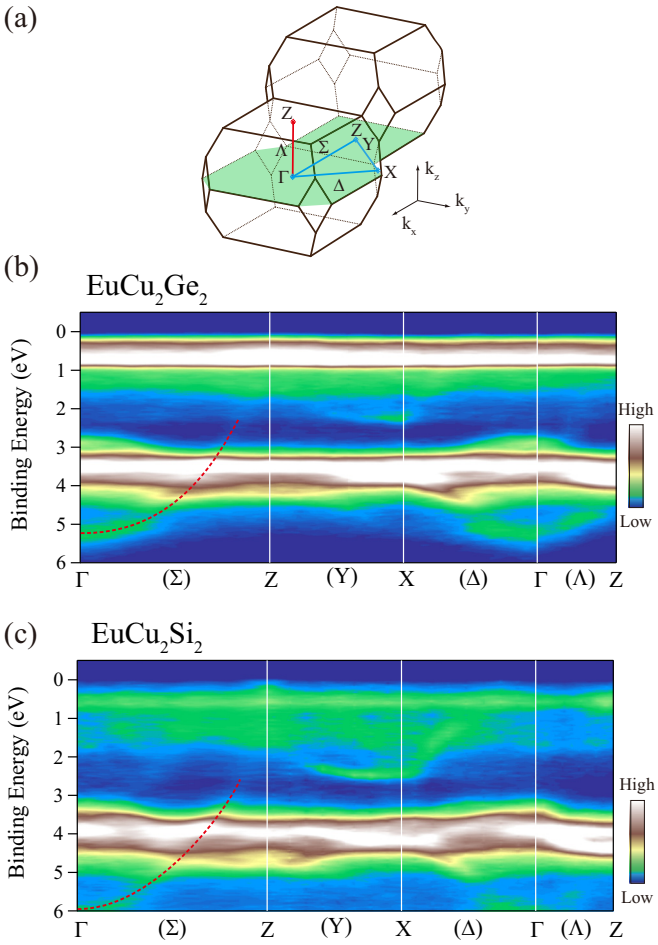

FIG. 2. (a) Brillouin zone of $EuCu_2Ge_2$ and $EuCu_2Si_2$, which have a body-centered tetragonal crystal structure. Intensity plots of ARPES spectra measured along the high-symmetry lines of (b) $EuCu_2Ge_2$ and (c) $EuCu_2Si_2$. The ARPES spectra in the Γ-X-Z plane, shown by the green plane, in the Brillouin zone were obtained by ARPES measurements at constant photon energies of $h\nu = 680$ and 710 eV for $EuCu_2Ge_2$ and $EuCu_2Si_2$, respectively. The ARPES spectra along the Γ-(Λ)-Z line were obtained by $h\nu$-dependent ARPES from 670 to 740 and 694 to 778 eV for $EuCu_2Ge_2$ and $EuCu_2Si_2$, respectively. The red dashed lines are guides to the eyes.

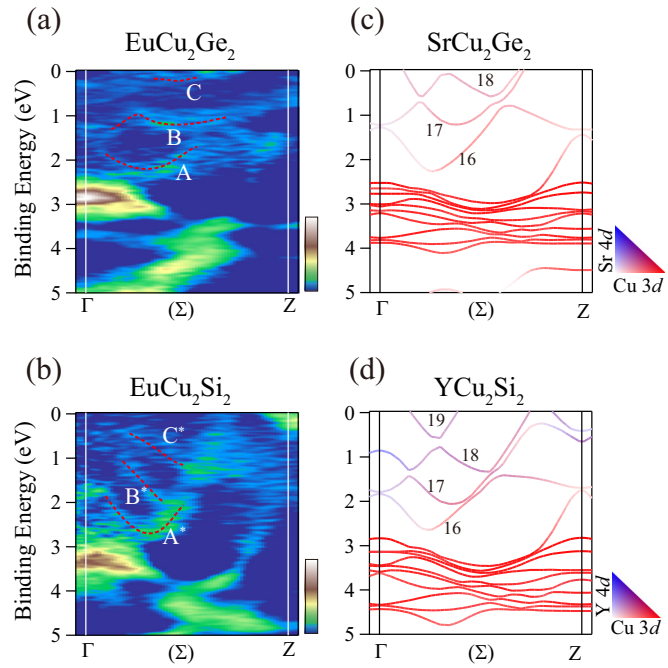

FIG. 3. ARPES spectra along the Γ-(Σ)-Z line measured at $h\nu = 680$ and 710 eV for (a) $EuCu_2Ge_2$ and (b) $EuCu_2Si_2$. We normalized these spectra by the integrated intensity of each momentum distribution curve. The red dashed lines are guides to the eyes. Calculated band structures of (c) $SrCu_2Ge_2$ and (d) YCu_2Si_2 along the Γ-(Σ)-Z line. The color of each band represents the contributions of the Cu 3d and Sr 4d (Y 4d) states for $SrCu_2Ge_2$ (YCu_2Si_2).

distribution function has the same value within each momentum distribution curve. In the $EuCu_2Ge_2$ spectrum, there are three bands, as indicated by red dashed lines in Fig. 3(a). They are designated A, B, and C. As shown in Fig. 3(b), similar bands, named A^*, B^*, and C^*, can be seen in the spectrum of $EuCu_2Si_2$; these bands are located at slightly higher binding energies. Note that we cannot resolve any valence-band splitting due to the hybridization with the Eu^{2+} components in Figs. 3(a) and 3(b), which means that the energy scale of the hybridization is smaller than the energy resolution of the present ARPES experiments. The most striking difference between the band structures of $EuCu_2Ge_2$ and $EuCu_2Si_2$ can be seen near E_F at the Z point. An electron-pocket-like feature with strong intensity can be recognized in the spectrum of $EuCu_2Si_2$, whereas this feature is missing in the spectrum of $EuCu_2Ge_2$.

To understand the origin of the above-mentioned difference between the band structures of $EuCu_2Ge_2$ and $EuCu_2Si_2$, we performed band structure calculations of $SrCu_2Ge_2$ and YCu_2Si_2 based on a Dirac-type linearized augmented-plane-wave method within a local-density approximation [29]. The former calculation corresponds to the Eu^{2+} state of $EuCu_2Ge_2$, assuming that the 4f electrons are localized and do not contribute to formation of the dispersive bands. The latter calculation corresponds roughly to the nearly Eu^{3+} state of $EuCu_2Si_2$ under the same assumption. Figures 3(c) and 3(d) show the calculated band structures of $SrCu_2Ge_2$ and YCu_2Si_2 along the Γ-(Σ)-Z line. The color of each band represents the contributions of the Cu 3d and Sr 4d (Y 4d) states for $SrCu_2Ge_2$ (YCu_2Si_2). The existence of bands 16, 17, and 18 near E_F is predicted for $SrCu_2Ge_2$. These bands correspond well to bands A, B, and C in the ARPES spectrum of $EuCu_2Ge_2$. Calculated bands 16, 17, and 18 of YCu_2Si_2 are shifted to higher binding energies compared to those of $SrCu_2Ge_2$, and band 19 is partially occupied. Calculated bands 16, 17, and 18 of YCu_2Si_2 seem to reproduce bands A^*, B^*, and C^* of $EuCu_2Si_2$, although band 19 is not well resolved in the present ARPES spectra. Our band structure calculations for $SrCu_2Ge_2$ and YCu_2Si_2 predict the presence of many highly dispersive valence bands, such as bands 16, 17, and 18, in the binding energy range from E_F to around 6 eV. These dispersive bands for $SrCu_2Ge_2$ (YCu_2Si_2) are derived mainly from Ge 4p (Si 3p), Cu 3d, and Sr 4d (Y 4d) orbitals. The difference between the calculated band structures of $SrCu_2Ge_2$ and YCu_2Si_2 can be ascribed to a difference in the

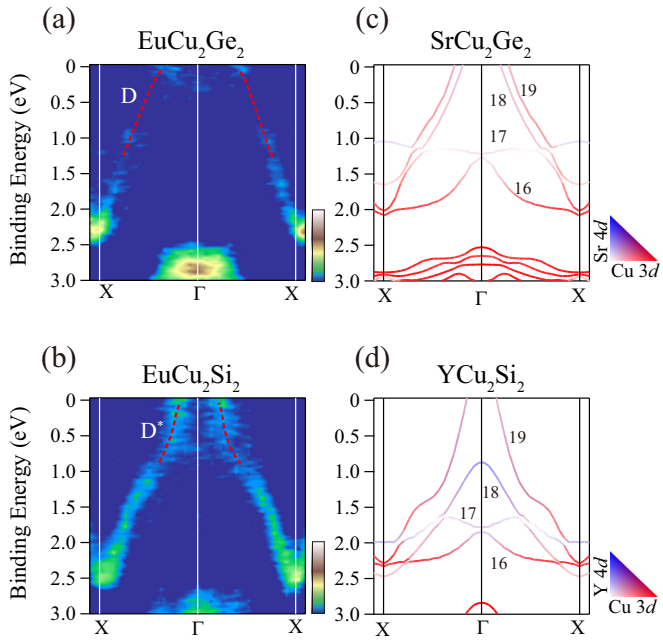

FIG. 4. ARPES spectra of (a) $EuCu_2Ge_2$ and (b) $EuCu_2Si_2$ measured at $h\nu = 680$ and 710 eV along the X-Γ-X line. We normalized these spectra by the integrated intensity of each momentum distribution curve. The red dashed lines are guides to the eyes. Corresponding calculated band structures of (c) $SrCu_2Ge_2$ and (d) YCu_2Si_2. The color of each band represents the contributions of the Cu $3d$ and Sr $4d$ (Y $4d$) states for $SrCu_2Ge_2$ (YCu_2Si_2).

number of valence electrons, which is due to an additional valence electron in YCu_2Si_2. On the other hand, we would like to stress that the difference between these band structure calculations cannot be understood by a simple rigid band model. This is because the Y $4d$ state of YCu_2Si_2 is selectively shifted toward the higher-binding-energy side compared to the Sr $4d$ state of $SrCu_2Ge_2$ due to the increased charge of the core of the Y atoms. In fact, calculated bands 16, 17, and 18 of YCu_2Si_2 have stronger Y $4d$ components compared to the Sr $4d$ components in the corresponding bands in $SrCu_2Ge_2$, as shown in Figs. 3(c) and 3(d). Accordingly, bands A^*, B^*, and C^* of $EuCu_2Si_2$ are expected to have stronger Eu $5d$ components than those of bands A, B, and C of $EuCu_2Ge_2$. It is noteworthy that the electron-pocket-like feature in Fig. 3(b) near E_F at the Z point is well explained by bands 17 and 18, and the absence of this feature in $EuCu_2Ge_2$ is consistent with the calculated band structure of $SrCu_2Ge_2$. Therefore, the overall band structures of $EuCu_2Ge_2$ and $EuCu_2Si_2$ and the difference between them seem to be reproduced by the calculations for $SrCu_2Ge_2$ and YCu_2Si_2. This indicates that the difference between the band structures of $EuCu_2Ge_2$ and $EuCu_2Si_2$ is ascribed to the charge transfer from the localized $4f$ states into the valence bands, which is caused by the change in Eu valence from a Eu^{2+} state toward a Eu^{3+} state.

The difference between the band structures of $EuCu_2Ge_2$ and $EuCu_2Si_2$ has been observed along the X-Γ-X line as well. Figures 4(a) and 4(b) show the ARPES spectra of $EuCu_2Ge_2$ and $EuCu_2Si_2$ along this line measured at $h\nu =$ 680 and 710 eV, respectively. The method for normalization of these spectra is the same as that in Figs. 3(a) and 3(b). As can be seen, holelike bands exist in both ARPES spectra, which are designated as D and D^*. They cross E_F, and band D^* has smaller Fermi momenta than band D. The calculated band structures of $SrCu_2Ge_2$ and YCu_2Si_2 are shown in Figs. 4(c) and 4(d), respectively. The calculation for $SrCu_2Ge_2$ predicts two holelike bands, 18 and 19, near E_F, and they seemingly correspond to band D of $EuCu_2Ge_2$; the intensity of band D is considered to be mainly due to band 19 because the Cu $3d$ contribution of band 19 is approximately double that of band 18. In the calculation for YCu_2Si_2, only band 19 crosses E_F, and therefore, this calculated band seems to correspond to band D^*. The absence of band 18 in the ARPES spectrum of $EuCu_2Si_2$ is possibly because of the smallness of the Cu $3d$ contribution. Band 16 is also missing in both Figs. 4(a) and 4(b) in spite of its relatively large Cu $3d$ contribution. One possible explanation for the absence of this band is that the intensity is suppressed by the photoemission structure factor, which originates from the interference effect between atomic orbitals with different positions in the unit cell [30]. As shown in Figs. 4(c) and 4(d), the Fermi momenta of calculated band 19 of YCu_2Si_2 are smaller than those of calculated band 19 of $SrCu_2Ge_2$, which is consistent with the behavior of experimental bands D and D^*. Accordingly, the difference between the band structures of $EuCu_2Ge_2$ and $EuCu_2Si_2$ along the X-Γ-X line is also consistent with the above-mentioned charge transfer from the localized $4f$ states to the valence bands.

Next, we discuss the shapes of the FSs of $EuCu_2Ge_2$ and $EuCu_2Si_2$. Figure 5(a) shows the photoemission intensity of $EuCu_2Ge_2$ integrated over $E_F \pm 50$ meV in the k_x-k_y plane, which was obtained by ARPES measurements at $h\nu = 680$ eV and represents the structure of the FSs in this plane. Complex spectral features, which imply the presence of several FSs, have been observed. We recognized a characteristic spectral intensity around the X point, as indicated by the white dashed line. The same image in the k_{xy}-k_z plane obtained by $h\nu$-dependent ARPES measurements is shown in Fig. 5(c). As indicated by the white dashed line in Fig. 5(c), there is a corrugated spectral intensity extending along the k_z direction, suggesting the presence of an open FS. The considerable dependence of this spectral intensity on k_z reflects the three-dimensionality of the FS shapes. One may point out that the intensity maps in Figs. 5(a) and 5(c) are not symmetric with respect to some high-symmetry points. This is possibly due to the aforementioned photoemission structure factor, with which the photoemission intensity changes between different Brillouin zones [30]. The corresponding calculated FSs of $SrCu_2Ge_2$ in the k_x-k_y and k_{xy}-k_z planes are shown in Figs. 5(b) and 5(d), respectively, and their three-dimensional shapes are shown in Fig. 5(e). In this calculation, band 17 forms a closed-hole FS centered at the Z point, and bands 18 and 19 form open-hole and -electron FSs. Note that the total volume of the calculated hole FSs is equal to that of the calculated electron FSs because $SrCu_2Ge_2$ is a compensated metal whose unit cell has an even number of electrons. We found that the spectral intensity around the X point, indicated by the white dashed line in the k_x-k_y plane, is well explained by the calculated FSs of band 19. Although the shapes of the FSs of bands 17 and 18 are not well resolved in the experimental intensity map in the

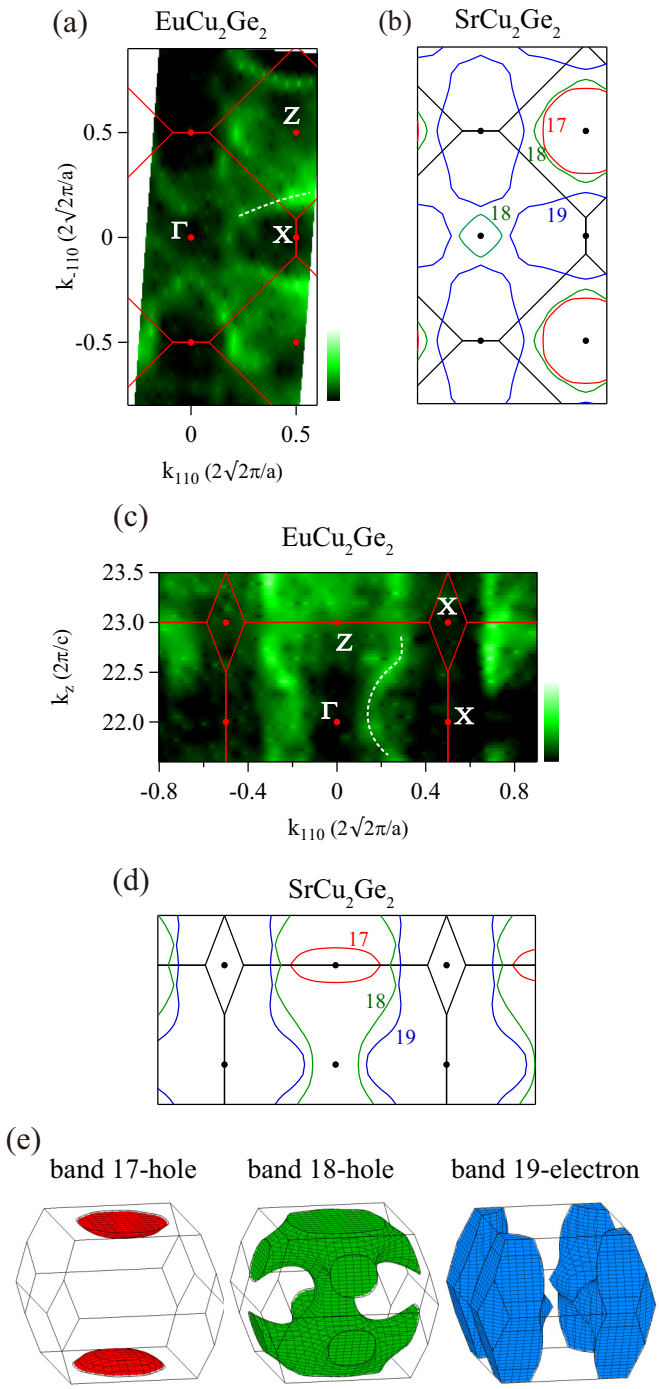

FIG. 5. FS images of $EuCu_2Ge_2$ in the (a) k_x-k_y and (c) k_{xy}-k_z planes obtained by ARPES measurements at $h\nu = 680$ eV and $h\nu$-dependent ARPES measurements, respectively. The white dashed lines are guides to the eyes. Corresponding calculated FSs of $SrCu_2Ge_2$ in the (b) k_x-k_y and (d) k_{xy}-k_z planes. (e) Three-dimensional shapes of the calculated FSs.

k_x-k_y plane, the observed spectral intensity around the Γ and Z points could be due to these FSs. In addition, the corrugated spectral intensity extending along the k_z direction in Fig. 5(c) seems to be reasonably explained by the FSs of band 18 and/or band 19. Accordingly, the experimental FS images are considered consistent with the calculation for $SrCu_2Ge_2$.

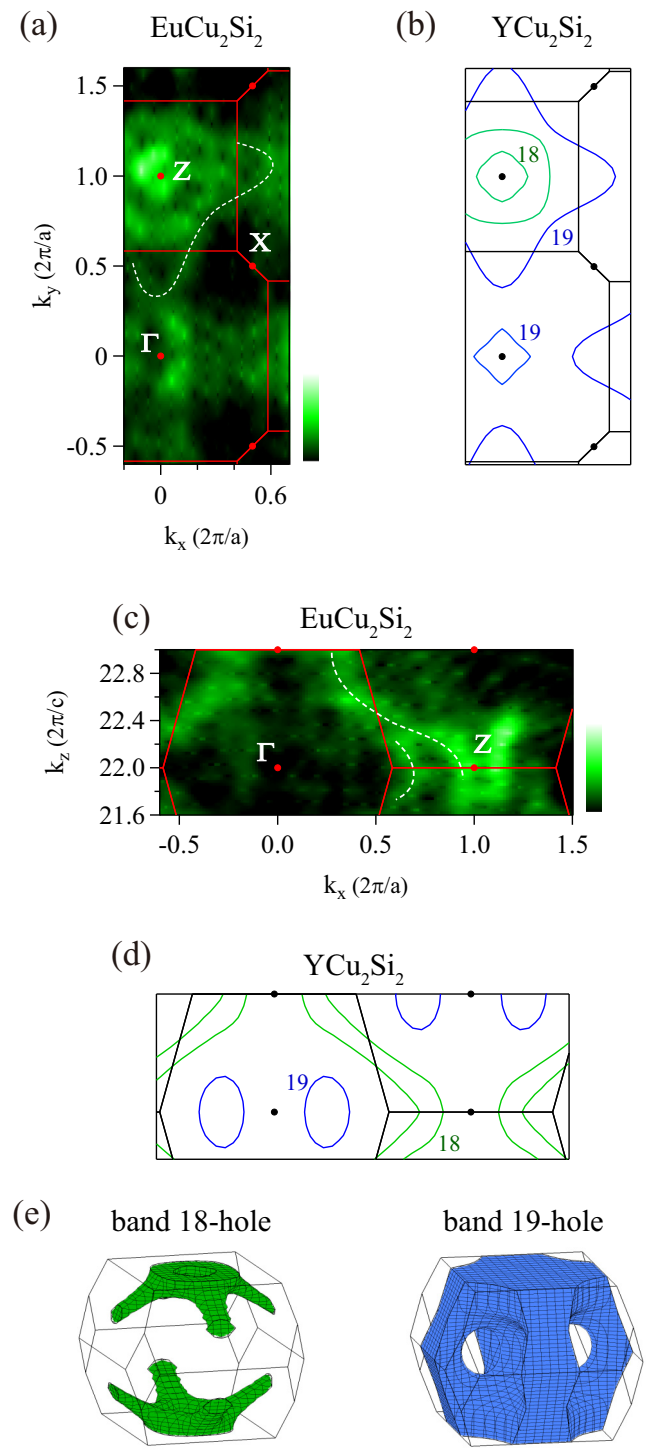

FIG. 6. FS images of $EuCu_2Si_2$ in the (a) k_x-k_y and (c) k_x-k_z planes obtained by ARPES measurements at $h\nu = 710$ eV and $h\nu$-dependent ARPES measurements, respectively. The white dashed lines are guides to the eyes. Corresponding calculated FSs of YCu_2Si_2 in the (b) k_x-k_y and (d) k_x-k_z planes. (e) Three-dimensional shapes of the calculated FSs.

The photoemission intensity integrated over $E_F \pm 50$ meV for $EuCu_2Si_2$ in the k_x-k_y plane, which is obtained by ARPES measurements at $h\nu = 710$ eV, is shown in Fig. 6(a). It has several characteristic spectral features, suggesting the

existence of several FSs, as in the FS images for $EuCu_2Ge_2$. For example, an enhanced intensity at the Z point is seen, and there is a circle-shaped spectral intensity surrounding the Z point. One can also notice another circle-shaped Γ-concentric spectral intensity. Moreover, we recognized a characteristic spectral feature centered at the Z point, as indicated by the white dashed line. Figure 6(c) displays the same image in the k_x-k_z plane obtained by $h\nu$-dependent ARPES measurements. As indicated by the white dashed lines, there exists a highly corrugated spectral intensity extending along the k_z direction. Figures 6(b) and 6(d) show the calculated FSs of YCu_2Si_2 in the k_x-k_y and k_x-k_z planes, and their three-dimensional shapes are shown in Fig. 6(e). The calculated FSs of YCu_2Si_2 are markedly different from those of $SrCu_2Ge_2$ because of the aforementioned difference in electron number. As can be seen in Figs. 6(b), 6(d) and 6(e), bands 18 and 19 constitute complex open FSs. We have found that the enhanced intensity at the Z point in the k_x-k_y plane corresponds well to the calculated FSs of band 18. The Z-concentric circle-shaped spectral intensity in the same plane also agrees with the calculated FSs of band 18, although the size of this spectral intensity is slightly larger than the calculated FSs of band 18. The spectral intensity surrounding the Γ point can be explained by the FS of band 19. Band 19 also explains the characteristic spectral feature indicated by the white dashed line in the k_x-k_y plane. Moreover, the highly corrugated spectral intensity indicated by the white dashed lines in Fig. 6(c) agrees well with the calculated FS of band 18, although the FSs of band 19 are not clearly seen in Fig. 6(c). Hence, we consider that the overall shapes of the FSs of $EuCu_2Si_2$ are consistent with the band structure calculation, as in the case of $EuCu_2Ge_2$. This result is reminiscent of de Haas–van Alphen (dHvA) experiments performed on the nearly trivalent Eu compound $EuCo_2Si_2$ [31]. In this dHvA study, the dHvA branches are well explained by the band structure calculation of YCo_2Si_2, revealing a similarity in FS properties between a nearly trivalent Eu compound and an Y-based compound, as in the present study. We have clarified that the FSs of $EuCu_2Ge_2$ and $EuCu_2Si_2$ are consistent with the calculations for $SrCu_2Ge_2$ and YCu_2Si_2, whose FSs are very different from each other. This further supports the above-mentioned assertion that the difference in the electronic structures between $EuCu_2Ge_2$ and $EuCu_2Si_2$ is caused by a charge transfer from the localized $4f$ states to the valence bands.

Next, we discuss the role of the hybridization between the $4f$ and the valence-band states. As pointed out in the Introduction, the observation of the heavy-fermion behavior in $EuCu_2(Ge_{1-x}Si_x)_2$ around x_c underlines the importance of the hybridization between the $4f$ and the valence-band states in this system [11,12]. Meanwhile, the present ARPES spectra and FS images of $EuCu_2Ge_2$ and $EuCu_2Si_2$ agree well with the band structure calculations of $SrCu_2Ge_2$ and YCu_2Si_2, which correspond to $4f$-localized states. In addition, we cannot resolve any valence-band splitting due to the hybridization with the $4f^6$ final-state multiplet in the present ARPES spectra. This absence of the valence-band splitting in our spectra is most likely due to the smallness of the energy scale of the hybridization. In fact, high-resolution ARPES experiments using low-energy photons ($h\nu = 34$ to 55 eV) performed on $EuNi_2P_2$ have revealed that the energy scale of the hybridization between the $4f^6$ final-state multiplet components and the valence bands is considerably smaller than the energy resolution of our experiments [32]. Moreover, according to this study, the energy scale of the hybridization further decreases for the multiplet components located near E_F, and thus, the positions of the Fermi momenta are little affected by the hybridization. We believe that the overall structures of the valence bands near E_F and the FSs of $EuCu_2Ge_2$ and $EuCu_2Si_2$ determined from our ARPES experiments are hardly affected by the $4f^6$ final-state multiplet because the γ values of $EuCu_2Ge_2$ and $EuCu_2Si_2$ are smaller than that for $EuNi_2P_2$, indicating that the valence bands near E_F of the former compounds are less affected by the final-state multiplet than the latter.

In the present study, we clarified that the FSs and the band structure near E_F of $EuCu_2Si_2$ differ markedly from those of $EuCu_2Ge_2$, and this difference can be explained by a charge transfer from the localized $4f$ states to other valence bands. This suggests that the band structure near E_F in $EuCu_2(Ge_{1-x}Si_x)_2$ is affected by the change in the Eu valence. The presence of the heavy-fermion state is confirmed around x_c by the specific-heat, resistivity, and magnetic susceptibility measurements as described in the Introduction [11,12]. Note that the Eu valence rapidly evolves with x around x_c, reflecting that the band structure near E_F changes markedly with x in the same x range. Thus, direct observation of the band structure near E_F around x_c by conducting higher-energy-resolution ARPES experiments will provide crucial information about the nature of the heavy-fermion state in the $EuCu_2(Ge_{1-x}Si_x)_2$ system.

IV. CONCLUSION

The electronic states of the Bridgman-grown single crystals of $EuCu_2Ge_2$ and $EuCu_2Si_2$ have been investigated by AIPES and ARPES experiments using bulk-sensitive soft x rays. A pronounced Eu^{2+} peak and the absence of Eu^{3+} components in the AIPES spectrum of $EuCu_2Ge_2$ show a divalent nature of the Eu ions. By contrast, the coexistence of Eu^{2+} and Eu^{3+} components in the AIPES spectrum of $EuCu_2Si_2$ indicates a mixed-valence nature, and the Eu valence is estimated to be 2.79. This Eu valence value is close to that estimated by XAS measurements performed on arc-melted $EuCu_2Si_2$ samples. The electronic states of In-flux-grown single crystals of $EuCu_2Ge_2$ and $EuCu_2Si_2$ were also investigated by AIPES experiments. We found the Eu ions of both the In-flux-grown samples to be in the divalent state, in contrast to those of the Bridgman-grown samples. This result is consistent with previous magnetic susceptibility and Mössbauer experiments performed on the In-flux-grown samples. The ARPES experiments performed on the Bridgman-grown $EuCu_2Ge_2$ and $EuCu_2Si_2$ single crystals showed that the two compounds differ markedly in terms of the band structure near E_F and the shapes of FSs. We clarified that the band structures and the FSs of $EuCu_2Ge_2$ and $EuCu_2Si_2$ are well explained by the band structure calculations of $SrCu_2Ge_2$ and YCu_2Si_2. Accordingly, the charge transfer from the localized $4f$ states to the valence bands, which is associated with the change in the valence state of Eu ions, seemingly accounts for the observed difference in the band structures between $EuCu_2Ge_2$ and $EuCu_2Si_2$.

ACKNOWLEDGMENTS

This work was performed under Proposals No. 2018A3811 and No. 2018B3811 at SPring-8 BL23SU. The present work was financially supported by JSPS KAKENHI Grants No. JP18H043298, JP17K05547, JP18K03553, and JP16H01084 and a grant of academic research from Hyogo Science and Technology Association.

[1] G. R. Stewart, Rev. Mod. Phys. **73**, 797 (2001).
[2] G. R. Stewart, Rev. Mod. Phys. **78**, 743 (2006).
[3] P. Gegenwart, Q. Si, and F. Steglich, Nat. Phys. **4**, 186 (2008).
[4] C. Pfleiderer, Rev. Mod. Phys. **81**, 1551 (2009).
[5] A. Mitsuda, S. Hamano, N. Araoka, H. Yayama, and H. Wada, J. Phys. Soc. Jpn. **81**, 023709 (2012).
[6] F. Honda, K. Okauchi, A. Nakamura, D. Li, D. Aoki, H. Akamine, Y. Ashitomi, M. Hedo, T. Nakama, and Y. Ōnuki, J. Phys. Soc. Jpn. **85**, 063701 (2016).
[7] H.-J. Hesse, R. Lübbers, M. Winzenick, H. Neuling, and G. Wortmann, J. Alloys Compd. **246**, 220 (1997).
[8] A. Nakamura, T. Nakama, K. Uchima, N. Arakaki, C. Zukeran, S. Komesu, M. Takeda, Y. Takaesu, D. Nakamura, M. Hedo, K. Yagasaki, and Y. Uwatoko, J. Phys.: Conf. Ser. **400**, 032106 (2012).
[9] G. Dionicio, H. Wilhelm, Z. Hossain, and C. Geibel, Phys. B (Amsterdam, Neth.) **378–380**, 724 (2006).
[10] A. Nakamura, T. Uejo, F. Honda, T. Takeuchi, H. Harima, E. Yamamoto, Y. Haga, K. Matsubayashi, Y. Uwatoko, M. Hedo, T. Nakama, and Y. Ōnuki, J. Phys. Soc. Jpn. **84**, 124711 (2015).
[11] S. Fukuda, Y. Nakanuma, J. Sakurai, A. Mitsuda, Y. Isikawa, F. Ishikawa, T. Goto, and T. Yamamoto, J. Phys. Soc. Jpn. **72**, 3189 (2003).
[12] Z. Hossain, C. Geibel, N. Senthilkumaran, M. Deppe, M. Baenitz, F. Schiller, and S. L. Molodtsov, Phys. Rev. B **69**, 014422 (2004).
[13] S. Doniach, Phys. B (Amsterdam, Neth.) **91**, 231 (1977).
[14] P. A. Alekseev, K. S. Nemkovski, J.-M. Mignot, V. N. Lazukov, A. A. Nikonov, A. P. Menushenkov, A. A. Yaroslavtsev, R. I. Bewley, J. R. Stewart, and A. V. Gribanov, J. Phys.: Condens. Matter **24**, 375601 (2012).
[15] K. S. Nemkovski, D. P. Kozlenko, P. A. Alekseev, J.-M. Mignot, A. P. Menushenkov, A. A. Yaroslavtsev, E. S. Clementyev, A. S. Ivanov, S. Rols, B. Klobes, R. P. Hermann, and A. V. Gribanov, Phys. Rev. B **94**, 195101 (2016).
[16] E. R. Bauminger, D. Froindlich, I. Nowik, S. Ofer, I. Felner, and I. Mayer, Phys. Rev. Lett. **30**, 1053 (1973).
[17] P. G. Pagliuso, J. L. Sarrao, J. D. Thompson, M. F. Hundley, M. S. Sercheli, R. R. Urbano, C. Rettori, Z. Fisk, and S. B. Oseroff, Phys. Rev. B **63**, 092406 (2001).
[18] J.-S. Rhyee, B. K. Cho, and H. C. Ri, J. Appl. Phys. **93**, 8346 (2003).
[19] Z. Hossain, C. Geibel, H. Q. Yuan, and G. Sparn, J. Phys.: Condens. Matter **15**, 3307 (2003).
[20] P. Wang, Z. M. Stadnik, J. Żukrowski, B. K. Cho, and J. Y. Kim, Phys. Rev. B **82**, 134404 (2010).
[21] W. Iha, T. Yara, Y. Ashitomi, M. Kakihana, T. Takeuchi, F. Honda, A. Nakamura, D. Aoki, J. Gouchi, Y. Uwatoko, T. Kida, T. Tahara, M. Hagiwara, Y. Haga, M. Hedo, T. Nakama, and Y. Ōnuki, J. Phys. Soc. Jpn. **87**, 064706 (2018).
[22] A. Sekiyama, T. Iwasaki, K. Matsuda, Y. Saitoh, Y. Ōnuki, and S. Suga, Nature (London) **403**, 396 (2000).
[23] S. Tanuma, C. J. Powell, and D. R. Penn, Surf. Interface Anal. **43**, 689 (2011).
[24] Y. Saitoh, Y. Fukuda, Y. Takeda, H. Yamagami, S. Takahashi, Y. Asano, T. Hara, K. Shirasawa, M. Takeuchi, T. Tanaka, and H. Kitamura, J. Synchrotron Radiat. **19**, 388 (2012).
[25] S.-i. Fujimori, M. Kobata, Y. Takeda, T. Okane, Y. Saitoh, A. Fujimori, H. Yamagami, Y. Matsumoto, E. Yamamoto, N. Tateiwa, and Y. Haga, Phys. Rev. B **96**, 125117 (2017).
[26] F. Gerken, Ph.D. thesis, University of Hamburg, 1982.
[27] J. Yeh and I. Lindau, At. Data Nucl. Data Tables **32**, 1 (1985).
[28] W. D. Schneider, C. Laubschat, G. Kalkowski, J. Haase, and A. Puschmann, Phys. Rev. B **28**, 2017 (1983).
[29] H. Yamagami, J. Phys. Soc. Jpn. **67**, 3176 (1998).
[30] H. Daimon, S. Imada, H. Nishimoto, and S. Suga, J. Electron Spectrosc. Relat. Phenom. **76**, 487 (1995).
[31] Y. Ōnuki, A. Nakamura, D. Aoki, M. Boukahil, Y. Haga, T. Takeuchi, H. Harima, M. Hedo, and T. Nakama, J. Phys.: Conf. Ser. **592**, 012049 (2015).
[32] S. Danzenbächer, D. V. Vyalikh, Y. Kucherenko, A. Kade, C. Laubschat, N. Caroca-Canales, C. Krellner, C. Geibel, A. V. Fedorov, D. S. Dessau, R. Follath, W. Eberhardt, and S. L. Molodtsov, Phys. Rev. Lett. **102**, 026403 (2009).